NASA Technical Memorandum 78423

Dust Storms on Mars: Considerations and Simulations

Ronald Greeley
University of Santa Clara, Moffett Field, California

Bruce R. White
University of California, Davis, California

James B. Pollack
Ames Research Center, Moffett Field, California

James D. Iversen
Iowa State University, Ames, Iowa

Rodman N. Leach
University of Santa Clara, Moffett Field, California

National Aeronautics
and Space Administration

**Scientific and Technical
Information Office**

1977

DUST STORMS ON MARS: CONSIDERATIONS AND SIMULATIONS

R. Greeley,* B. R. White,† J. B. Pollack,‡ J. D. Iversen,§ and R. N. Leach*

SUMMARY

Aeolian processes are important in modifying the surface of Mars at present, and appear to have been significant in the geological past. Aeolian activity includes local and global dust storms, the formation of erosional features such as yardangs and depositional features such as sand dunes, and the erosion of rock and soil. As a means of understanding aeolian processes on Mars, an investigation is in progress that includes laboratory simulations, field studies of Earth analogs, and interpretation of spacecraft data. This report describes the Martian Surface Wind Tunnel (MARSWIT), an experimental facility established at NASA-Ames Research Center, and presents some results of the general investigation. Experiments dealing with wind speeds and other conditions required for the initiation of particle movement on Mars are described and considerations are given to the resulting effectiveness of aeolian erosion.

INTRODUCTION

For many years, Earth-based telescopic observations of Mars have revealed surface markings that change size, shape, and position with time, apparently in response to changes in the martian seasons. Although many origins have been attributed to these markings – including notions that they could be related to biological activity – in recent years it has become apparent that they are the result of atmospheric phenomena, including cloud formation and dust storm activity. This report considers some basic aspects of the martian dust storms and focuses primarily on the conditions for initiating particle movement by the wind with discussions based mainly on laboratory simulations.

We will first briefly review the current understanding of martian dust storms, then describe the experimental facility established at NASA-Ames Research Center to simulate martian aeolian activity, and then discuss the initial results obtained from this facility. Finally, we will discuss the implications of these results in terms of the geological history of Mars and of aeolian activity in general.

*University of Santa Clara at NASA Ames Research Center, M/S 245-5, Moffett Field, Calif. 94035.
†Mechanical Engineering Department, University of California, Davis, Calif. 95616.
‡National Aeronautics and Space Administration, Ames Research Center, Moffett Field, Calif. 94035.
§Department of Aerospace Engineering, Iowa State University, Ames, Iowa 50010.

MARTIAN DUST STORMS

More than one hundred years of observations of Mars have produced an impressive catalog documenting the changing patterns on that planet. In recent years staff at several observatories have closely followed the initiation and growth of global martian dust storms. Summarizing from reference 1, these observations show that major dust storms typically originate in three general areas of Mars - Hellespontus, Noachis, and Solis Planum - all elevated plateaus that are between 20° and 40° S latitude (fig. 1); Viking results are showing that local dust storms can occur in many other areas as well. Major storms typically begin near or slightly before the time of southern hemisphere solstice (close to perihelion), at the start of martian southern hemisphere summer, or late spring; however, some years there are no major dust storms.

The major storms appear to go through three phases. In phase I, lasting about five days, the storms begin as bright spots or cores, about 400 km or smaller in diameter. Phase II is the expansion of the storm which can last from about 35 to 70 days. Expansion takes place by having secondary cores develop around the primary cores of the first phase, until eventually the entire planet is affected. Moreover, the development of the storm path does not seem to be topographically related; for the largest storms, the entire planet may be totally obscured. Phase III marks the decay of the storm and lasts from 50 to 100 days. The first areas to clear are the poles and topographically high regions, such as the summits of the shield volcanoes. Although major dust storms do not occur every year (phase II – expansion -- may not fully develop), the occurrence is fairly frequent (ref. 1).

The Mariner 9 mission to Mars in 1971 provided the unique opportunity to observe dust storm activity at close range. Even before the spacecraft went into orbit, Earth-based observations showed that a major dust storm totally obscured the planet. Photographs obtained from Mariner 9 coupled with other data produced a wealth of new information on martian dust storms. Average particle size in the atmosphere was found to be less than 2 μm, or about the same as the particles carried over the Atlantic by major Saharan dust storms. The dust was found to be well mixed in the atmosphere to heights of 30 to 40 km and had the effect of raising the atmospheric temperature by as much as 50 K.

After the 1971 dust storm had essentially cleared, Mariner 9 photographed numerous local dust storms and a host of features that are attributed to aeolian processes (ref. 2 and others). Major findings include dune fields, polar laminated terrain (possibly composed of alternating layers of windblown dust and dust-ice mixtures) and yardangs. The most abundant type of aeolian feature, however, is the crater-streak (fig. 2), of which there are two types – dark streaks and light streaks. Dark streaks were seen to appear and change size and shape in a matter of weeks; light streaks remain relatively stable, taking years to change (ref. 3). Most dark streaks appear to represent areas where aeolian erosion has removed material, while some light streaks appear to represent dust deposits. The morphology of many streaks can be explained by the geometry of the wind flow field around and over craters and the resulting zones of wind-scour and deposition (refs. 4–8).

The Viking mission currently in progress is yielding even more data on martian aeolian processes. Two Viking Orbiters are producing photographs of the surface over large areas at resolutions substantially improved over Mariner 9, while two landers are obtaining the first pictures of the surface, making measurements of the wind speeds and directions, and obtaining data on the

Figure 1.– Shaded relief map of Mars (to 65°N and 65°S), showing Solis Planum, Noachis, and Hellespontus, areas where dust storms are observed to begin (Earth-based observations). Also shown are the Viking Lander 1 and 2 sites, and the area of major shield volcanoes, Tharsis Montes. Local dust storm activity shown in figures 5 and 6 are keyed to Argyre Planitia and the area northwest of Solis Planum, respectively (base map courtesy of the U.S. Geological Survey).

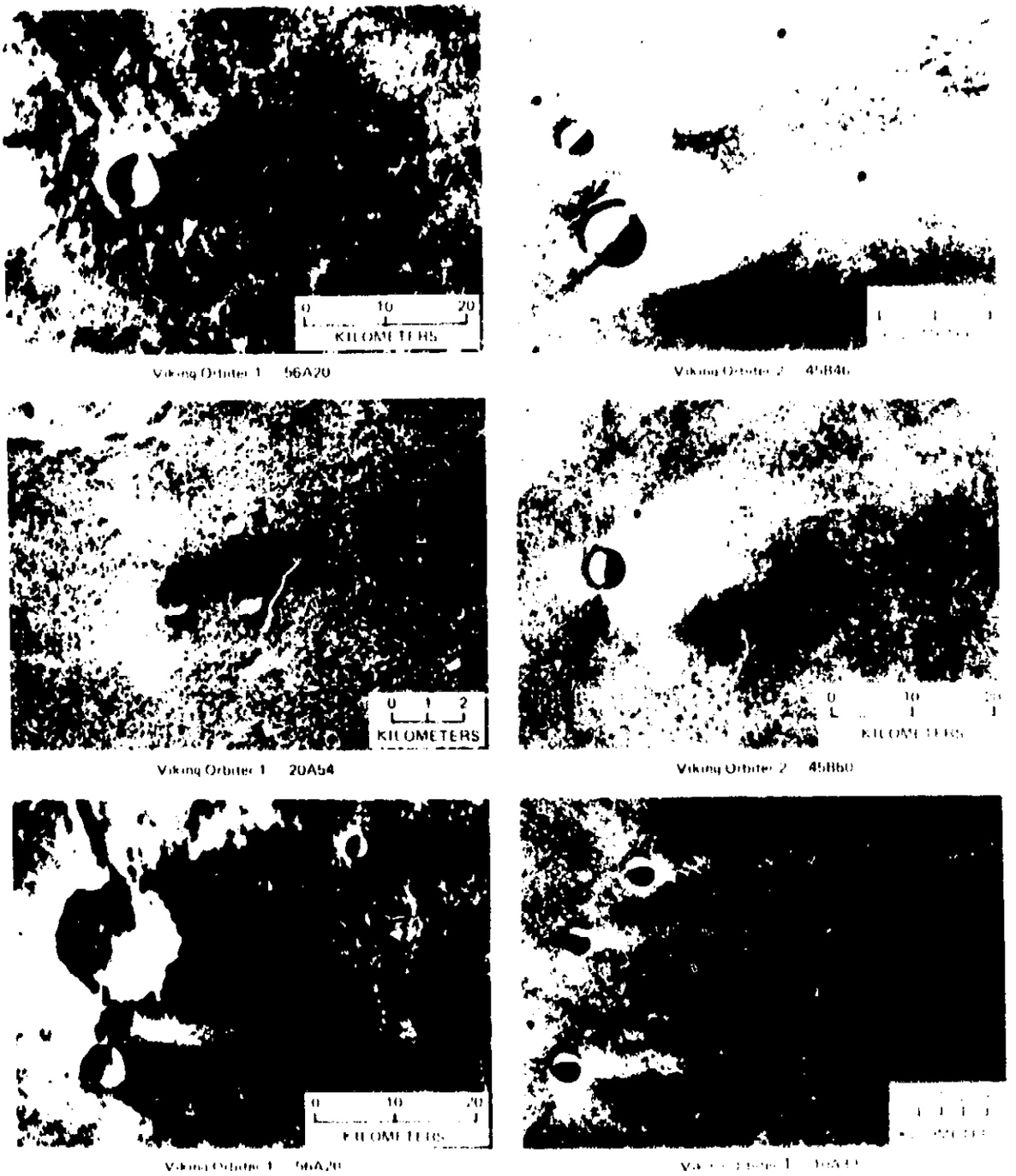

Figure 2.- Examples of several types of dark and light streaks associated with craters on Mars. Most dark streaks are generally considered to result from erosion of particles from the surface; some light streaks appear to be deposits of windblown particles.

atmospheric dust content for the two different landing sites in the northern hemisphere. Lander pictures at both sites show accumulation of windblown sediment as dune-forms (fig. 3), as well as evidence of aeolian erosion in the form of possible ventifacts (refs. 9 and 10). Orbiter pictures show newly discovered dune fields (fig. 4) and numerous crater streaks (ref. 11). Aeolian features

(a) Panoramic view of the surface of Mars from Viking Lander 1 in Chryse Planitia (see fig. 1). This image was taken in early morning (about 7:30 local time), August 3, 1977, and covers the view from the northeast at the left, to the southeast at the right. The large boulder at the left is about 1 by 3 m and is about 8 m from the spacecraft. The light-colored materials are deposits of windblown particles. The shape of the deposits suggest erosion by winds blowing from the upper left to the lower right (ref. 9).

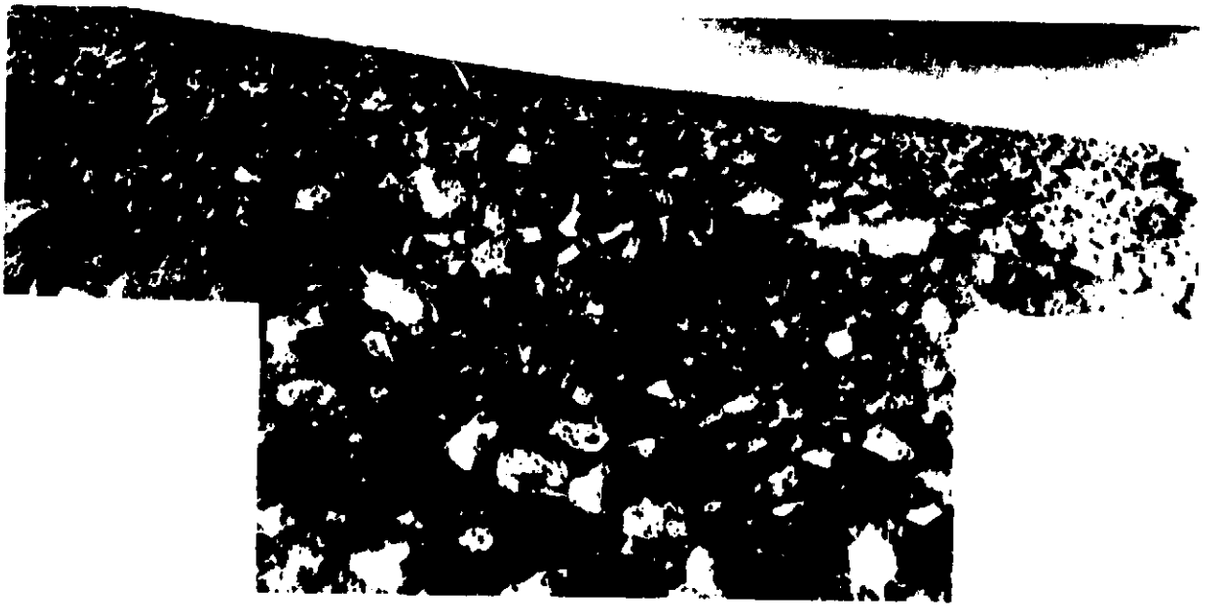

(b) View of martian surface from the Viking Lander 2 site in Utopia Planitia (see fig. 1), showing the rock-littered terrain and accumulations of fine-grained, windblown material. The horizon, which is some 3 km distant, is actually level; the tilt in the picture reflects the 8° tilt of the spacecraft and the manner in which the panoramic pictures are obtained (ref. 10).

Figure 3.– Views of martian surface from Viking.

Figure 4.– Viking Orbiter 1 view of a sand dune field contained within *Gangis Chasma*, a canyon of Vallis Marineris (see fig. 1). The field is about 50 km long and up to 20 km wide. Individual dunes are about 500 m across. The illumination is from the right toward the left.

observed from both orbit and on the ground will be monitored throughout the extended Viking mission into 1978 for observation and for correlation with the meteorology experiment results (refs. 12 and 13) and other Viking data. For example, local dust storms have been observed developing in the southern hemisphere (figs. 5 and 6) earlier than expected. By late martian spring (1977), most of the southern hemisphere was obscured, although the southern polar cap remained clear.

From Earth-based observations and numerous spacecraft missions, it is apparent that aeolian processes have played an important role in altering the surface of Mars. Knowledge of the physical and to some extent the chemical conditions that govern aeolian processes on Mars is paramount to our understanding of both the present environment of the planet and of its geological history.

In order to understand the nature of aeolian processes on Mars, a collaborative research program was established in 1972 that is a multidisciplinary effort involving a geologist, a planetary physicist, and aerodynamicists; it includes laboratory simulations (primarily wind-tunnel work), field studies of aeolian processes on Earth, and analyses of spacecraft data. Previous results from this program are reported in references 4–6 and 14–20.

Figure 5.– Viking Orbiter 2 photomosaic of dust storm (arrow) more than 300 km across inside the Argyre Basin (see fig. 1, Argyre Planitia).

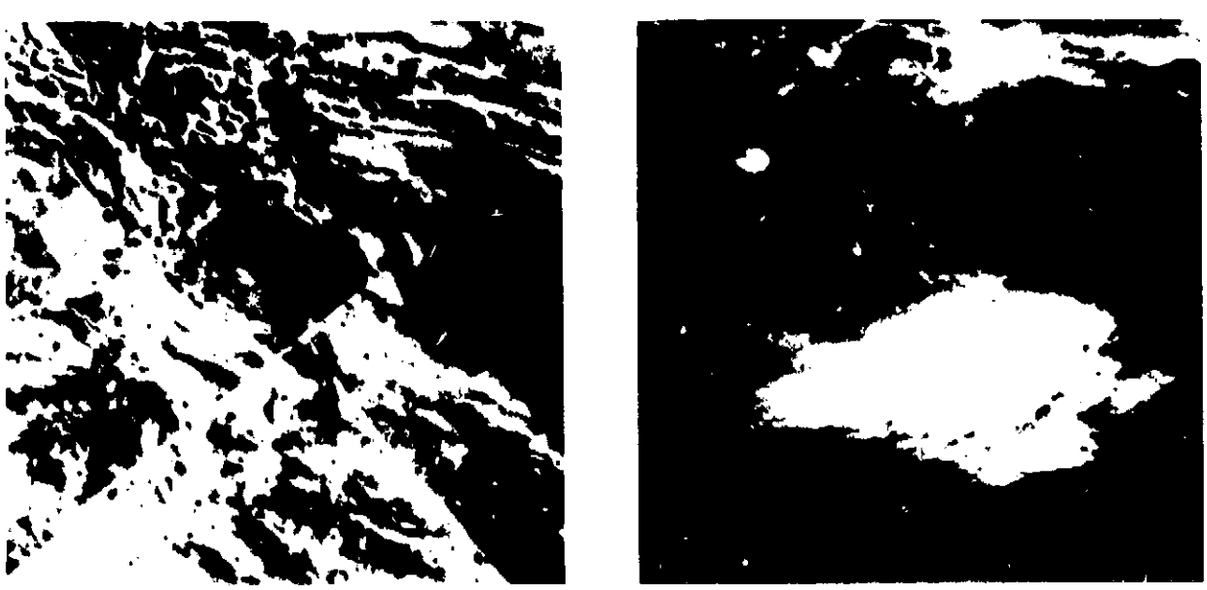

Figure 6.– Viking Orbiter views "before" (left) and "after" (right) of the region west of Vallis Marineris. The mosaic at left was taken July 31, 1976, and shows the surface in sharp detail; the picture at right was taken March 25, 1977, and shows the same area covered by diffuse clouds of water ice and dust.

THE MARTIAN SURFACE WIND TUNNEL (MARSWIT)

When the possibility of dust storms on Mars was first realized, many investigators attempted to predict the wind speeds and other conditions needed for martian winds to move fine-grained material. In most cases these investigators turned to the classic work of Bagnold (ref. 21) for the expressions describing aeolian processes and used the appropriate parameters for Mars in formulating their predictions. Assuming roughly analogous geological conditions of particle mineralogy, etc., the greatest problem in extrapolations from Earth to Mars are differences in temperature and atmospheric surface pressure and, to a much lesser extent, the two-thirds less gravity on Mars. The atmospheric surface pressure on Mars ranges from about 1 mb (100 Pa) on mountain tops to about 10 mb (1000 Pa) -- less than 1/100th that of the Earth -- with a nominal average of about 5.3 mb (530 Pa). Thus, the substantially "thinner" martian air, composed of 95 percent CO_2, 1--3 percent Ar, 2--3 percent N_2, 0.1--0.4 percent O_2 (ref. 22), must be blowing considerably faster than on Earth to accomplish the same effect, or to initiate particle movement. Unfortunately, imprecise knowledge of the effect of winds upon a loose particulate surface at low pressure makes extrapolations to Mars questionable. Widely divergent results for predictions of threshold wind speeds on Mars among various investigators prompted another approach, namely, experiments conducted at low pressure.

A low-pressure chamber at NASA-Ames Research Center, constructed in the early 1960's for a series of acoustic and structural tests at low pressure on rockets and since then vacated, was recommissioned to house the Martian Surface Wind Tunnel (MARSWIT). The chamber is a pentagon-shaped, concrete tower 30 m high, with a floor area of 164 m^2 and a total chamber volume of 4058 m^3 (fig. 7). The entire chamber can be evacuated to a minimum pressure of 3.8 mb (380 Pa) in a period of about 45 min using a steam-ejection system. A 7.6-m X 7.9-m door permits large experimental apparatus to be placed inside the chamber, and numerous plumbing and electrical fittings allow a variety of experiments to be conducted at low pressure. MARSWIT occupies the center of the chamber, as shown in figure 7.

MARSWIT (fig. 8) has an overall length of 14 m, with a 1.1-m^2 test section located 5 m from the entrance. The tunnel walls are constructed of 2.4-cm clear Plexiglas to enable ready viewing. The tunnel is driven by a network-ejector system consisting of 72 equally spaced 1.6-m nozzles located in the diffusor section. High pressure air (up to 9.86 kg/cm^2) is forced through the nozzles to induce flow of air through the tunnel. The maximum attainable free-stream airspeed is 13 m/sec at atmospheric pressure, increasing to 180 m/sec at 5 mb (500 Pa).

A naturally turbulent boundary layer occurs inside the tunnel at atmospheric pressures; however, at low pressures (corresponding to the range of martian surface pressures), it is necessary to "trip" the boundary layer in the entrance area to ensure that the boundary layer is turbulent. This is accomplished by means of vortex generators, consisting of small pebbles that are secured to the tunnel floor. The bed of pebbles extends approximately 3.5 m downstream from the entrance section. The wind tunnel boundary layer that is achieved corresponds to a neutrally stratified atmosphere in which the Monin-Obukhov stability length is infinite, hence the ratio of local surface roughness height to the stability length is zero. A finite value of the stability length could be achieved in the tunnel by heating or cooling the entire tunnel floor to obtain unstable or stable stratification, respectively.

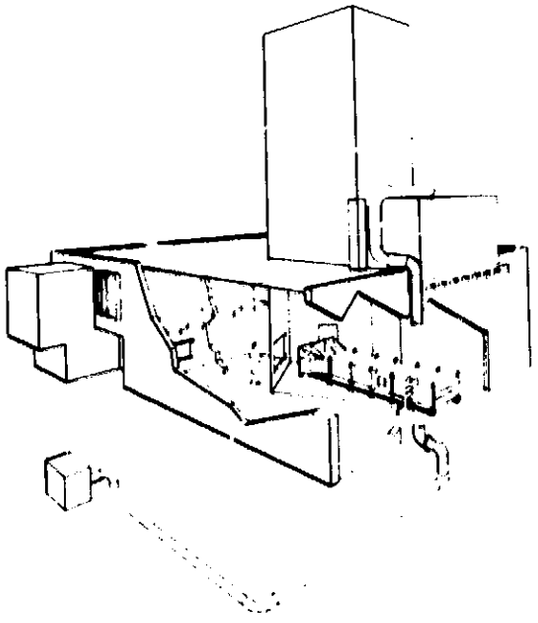

(a) Schematic diagram of the Martian Surface Wind Tunnel (MARSWIT), showing the low pressure chamber, the tunnel, and the control room.

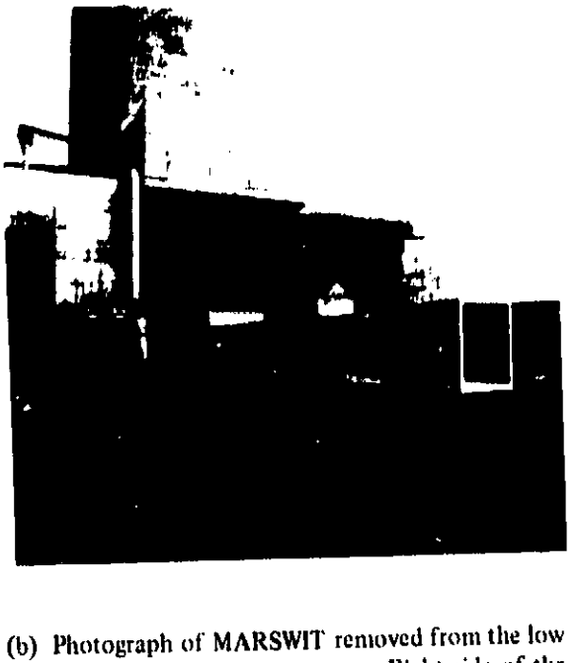

(b) Photograph of MARSWIT removed from the low pressure chamber for maintenance. Right side of the tunnel is the diffuser, exit end of the 13-m open circuit tunnel.

Figure 7.– Martian Surface Wind Tunnel (MARSWIT).

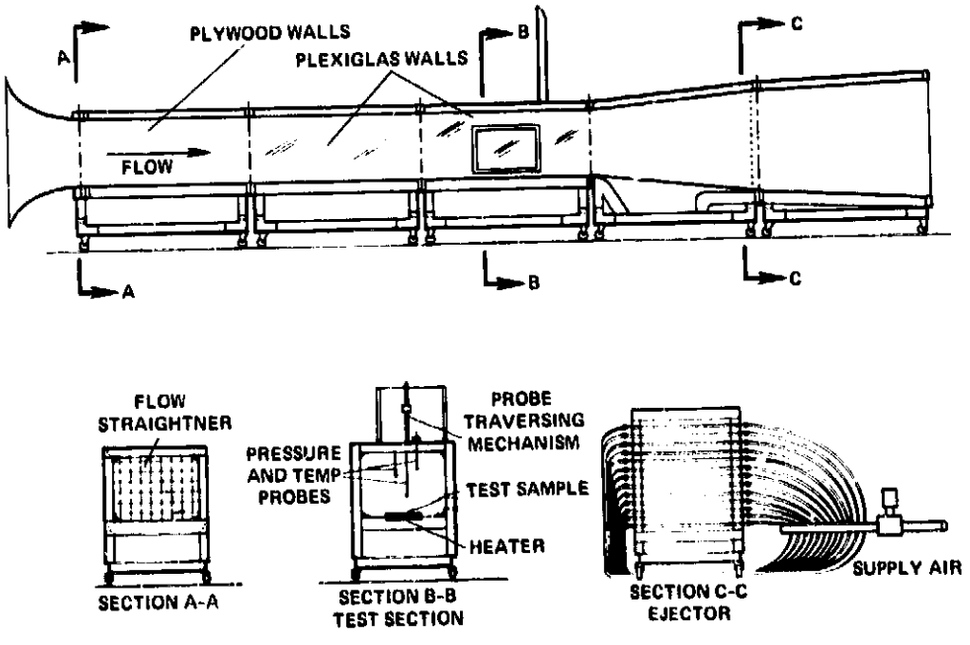

Figure 8.– Diagram of MARSWIT, showing entrance cone and flow straighteners (Section A-A), Test Section with various pressure probes (Section B-B), and diffuser-drive system (Section C-C).

THRESHOLD FRICTION SPEED EXPERIMENTS

Winds transport particles by surface traction, suspension, and saltation, the latter a term used to describe bouncing grains (derived from the Latin verb *saltare*, meaning "to leap or dance"). Material in traction moves very close to or on the surface by rolling, sliding, etc., whereas particles in suspension are held aloft by eddies of turbulent flow. Particles on Earth are most easily moved by the wind by saltation, with both surface creep and suspension resulting primarily from the impact of saltating grains. Thus most research, including most of that of Bagnold (ref. 21), has concentrated on the conditions of wind speed, surface roughness, etc., needed to initiate saltation. Bagnold defined two types of threshold — static threshold and dynamic threshold. Static threshold involves wind conditions needed to initiate grain movement for a bed of particles at rest. Dynamic threshold involves the initiation of grain movement for a bed that is being impacted by grains saltating from upwind; typically, somewhat lower wind speeds are needed for dynamic threshold than for static threshold. The threshold experiments described here are concerned with static threshold only.

The basic physics of windblown material is considered to be essentially the same whether it occurs on the surface of Earth or Mars. The primary difference is due to the comparatively thin martian atmosphere which requires much higher wind velocities to accomplish the same effect as on Earth. As the wind speed increases over a given surface, there is a minimum wind velocity (*v*) that is needed to initiate motion for particles of a given size and density. Corresponding to this minimum wind velocity is a threshold surface stress (τ_t) that is needed to set particles into motion. From this threshold stress, τ_t, a threshold friction velocity V_{*_t} may be defined as $\tau_t = \rho V_{*_t}$ where ρ is the fluid density. Experimentally V_{*_t} can be determined from knowledge of the vertical velocity structures above the surface.

Based on an evaluation of the important terrestrial parameters influencing the threshold friction velocity, Bagnold (ref. 21) derived the following expression for the threshold friction velocity on Earth

$$V_{*_t} = A\sqrt{\frac{(\rho_p - \rho)gD_p}{\rho}} \tag{1}$$

where ρ_p is particle density, g is acceleration due to gravity, D_p is the mean particle diameter, and A is an experimental coefficient. For particle motion to occur, the force caused by the horizontal wind stress must exceed the gravity force exerted on the particle. In the case of particles having densities much greater than the density of the fluid, equation (1) simplifies to

$$A = \frac{V_{*_t}}{\sqrt{(\rho_p g D_p/\rho)}} \tag{2}$$

The dimensionless quantity A appearing in these equations was assumed by Bagnold to be a unique function of only the particle friction Reynolds number B. B is defined as

$$B = \frac{V_{*_t} D_p}{\nu} \tag{3}$$

where ν is the kinematic viscosity. The parameter B provides a measure of how turbulent the flow is around the particle. In principle the determination of the function $A(B)$ is all that is necessary to obtain terrestrial values of V_{*_t} if the other parameters are known (e.g., D_p, ρ_p, ρ, g, and ν would ordinarily be specified). This function appears to predict accurately the values of V_{*_t} for Earth as long as $B \gtrsim 1$; however, it may not predict correct results for pressures lower than atmospheric, such as those on Mars.

Thus it is generally possible to predict the values of V_{*_t} for a range of conditions on Earth, and, for at least a first-order approximation, to predict V_{*_t} for Mars by using the appropriate martian values for the parameters involved. Accurate predictions, however, for Earth and especially for Mars involve several complicating factors. The original expressions for particle movement derived by Bagnold and amplified by others do not take into account such factors as lift forces, interparticle forces due to cohesion, electrostatic charges, etc., or the Magnus effect (a lift function) from spinning grains. Because these are important not only for understanding aeolian processes on Earth but are essential for extrapolations to Mars, some of these factors have been systematically investigated in the laboratory for one-atmosphere conditions and reported on earlier (refs. 4–5 and 18–20).

Despite the refinements that have been made in expressions describing wind threshold conditions on Earth, many fundamental questions remain regarding the behavior of windblown material under the low atmospheric pressure conditions on Mars; it was for this reason that MARSWIT was established. The first results from MARSWIT are described in a preliminary report by Greeley *et al.* (ref. 15); in this section, we describe more fully the experimental procedure and the threshold results for low pressure conditions.

There is a basic difference between the laboratory simulations and martian conditions. In the wind tunnel the working fluid is "Earth" air; however, on Mars the atmospheric gas is 95 percent carbon dioxide with lesser amounts of argon, nitrogen, and oxygen. The universal gas constant for air is $R = 0.287$ KJ/KgK, while for CO_2 it is 0.189 KJ/KgK. Hence, for air at a pressure of 5 mb (500 Pa) the gas density is 6.20×10^{-3} Kg/m^3, and for CO_2 at the same pressure the density is 9.42×10^{-3} Kg/m^3 or 52 percent more than air. Both densities were calculated for a constant temperature of 285 K. This represents a substantially larger density of the gas on the surface of Mars than comparable wind-tunnel tests have at the same pressures and temperatures. This will affect the forces on individual grains since the density of gas is directly related to the force. The absolute viscosity of air is approximately one-fifth greater than that of CO_2 at similar temperatures which also complicates the simulation. Thus MARSWIT results cannot be compared directly to similar martian surface conditions, and extrapolations must be developed to take into account these differences in order to make predictions for a wide range of surface pressures and temperatures on Mars.

Experimental Procedure

Threshold friction velocities V_{*_t} are typically plotted as a function of particle diameter D_p (fig. 9). Several different materials having a range of particle diameters and densities were tested in the MARSWIT. Each experiment consisted of placing a patch of particles in the tunnel test section, evacuating the chamber to its minimum pressure (~3.8 mb, or 380 Pa), and then increasing the wind speed through the tunnel until saltation was initiated. The free-stream wind speed was noted, correlated with a standard velocity profile for the tunnel at the given pressure and converted to a value of V_{*_t} (fig. 10). The chamber pressure was then increased and the procedure repeated for the higher value of surface pressure. This process was repeated for each particle test case, and threshold velocities were obtained as a function of pressures ranging from ~3.8 mb (380 Pa) to ~1000 mb (10^5 Pa).

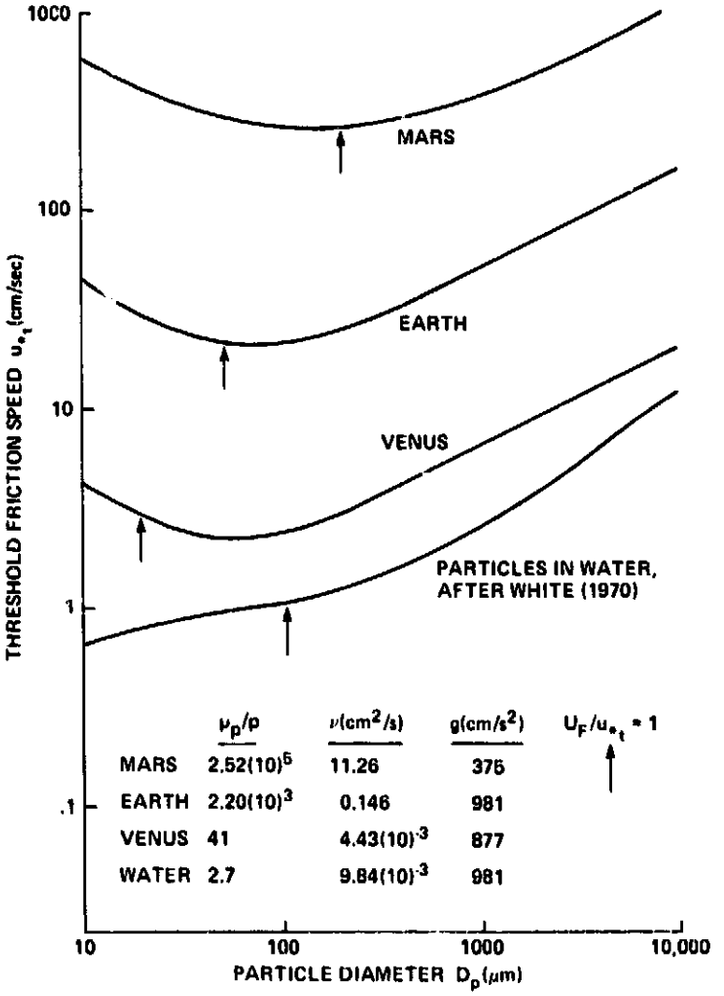

Figure 9.- Comparison of threshold friction speed vs particle diameter for Earth, Mars, Venus, and in liquid. In all cases except liquid, there is an "upturn" in the speed needed to set smaller grains in motion; thus, on each planet, there is an optimum particle size for movement by lowest winds (ref. 36).

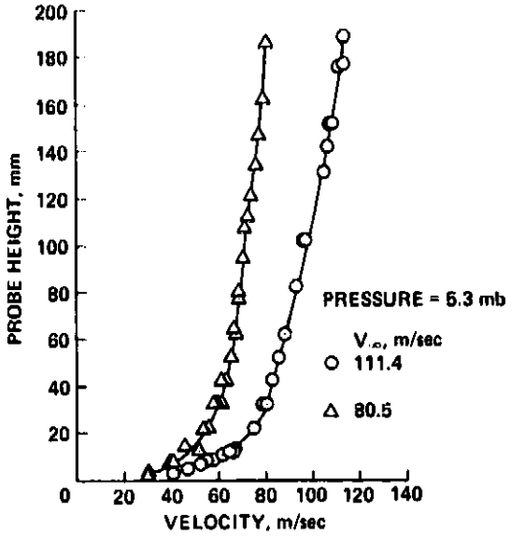

(a) Several velocities are run at each pressure. Height of boundary layer is determined.

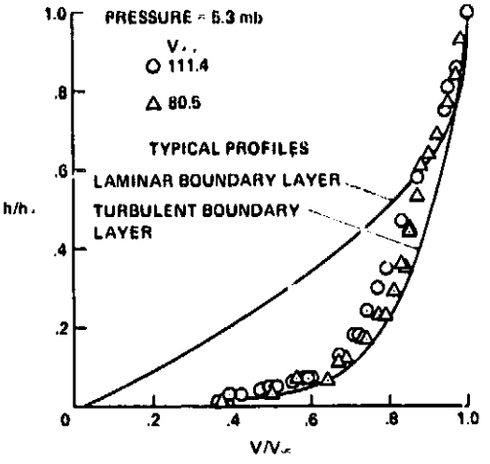

(b) Data is nondimensionalized and compared to standard profiles to insure that it is turbulent.

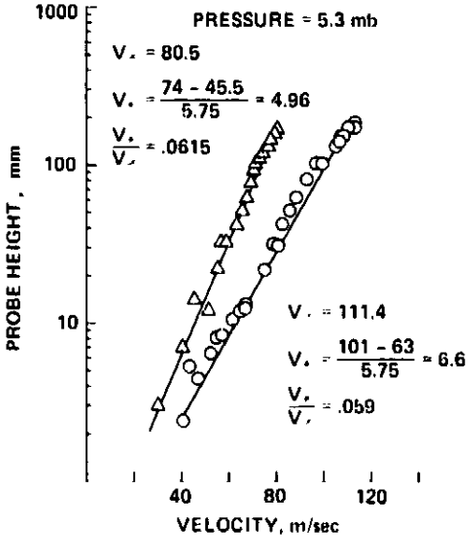

(c) Log slope is obtained to determine V_*, from relationship $V_* = (V_{100} - V_{10})/5.75$.

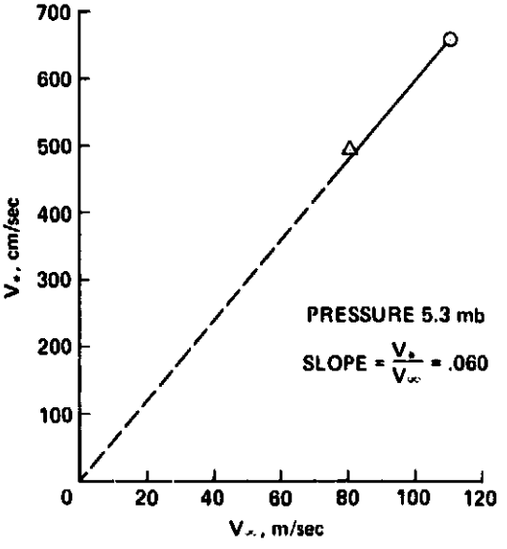

(d) The values of V_*/V_∞ are checked to ensure linearity.

Figure 10.– Determination of friction velocity, V_*, from boundary-layer profiles.

Test materials– Three kinds of materials were used in the threshold friction velocity experiments: silica microspheres, natural silt, and finely ground walnut shells. These materials (fig. 11) were selected because they afforded a variety of particle diameters and densities.

With knowledge of the geological environment of Mars derived from Mariner data and Viking Orbital information plus results obtained from the Viking Lander (refs. 9, 10, 23, and 24), windblown particles probably include weathered basalt fragments, clay materials, *duricrust* (crust-like material that may consist of agglomerates of fine particles), and perhaps certain "heavy"

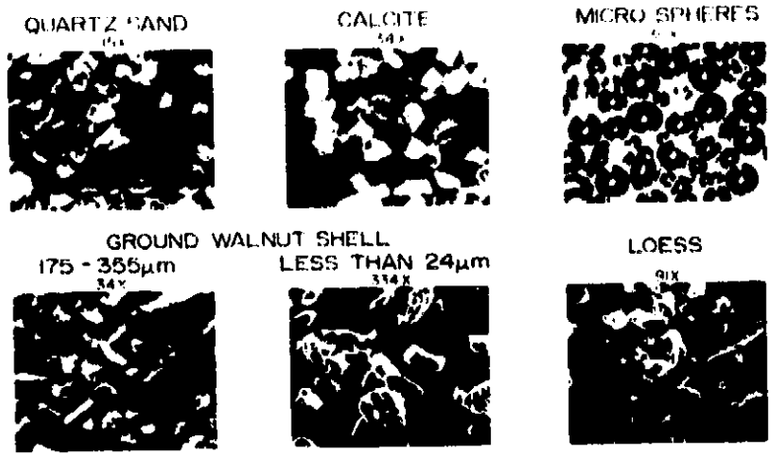

Figure 11.– Photomicrographs of some types of the particles used in threshold tests performed under low atmospheric pressures. Except for the losses, several size ranges of each type were run in the tests to provide a wide range of particle diameters and densities.

minerals such as magnetite (refs. 25 and 26). Thus the specific gravities of martian windblown particles probably range from less than 2 to more than 3. Gravity on Mars is 0.38 that of Earth; thus, less force is required to initiate particle lift and subsequent movement. Because gravity is a parameter that cannot be controlled in MARSWIT, some other means must be taken to simulate the lower gravity of Mars. For threshold simulations conducted on Earth, particles 0.38 as dense as those expected on Mars can be used to offset partly the difference in gravity. The ground walnut shells are considered appropriate since their density is about one-third that of possible windblown martian material and their shape is similar to natural windblown minerals (fig. 12). Thus the walnut shell material was used to derive most of the threshold velocity data for Mars; silica microspheres, silt, and other materials were used to provide a wide range of particle densities for derivation of "A" vs "B" relationships.

Cohesion resulting from water adsorbed on particles raises the threshold velocities above that for "dry" particles. To reduce the effect of this parameter, the test materials were heated in an oven to a temperature of about 425 K several hours prior to each run to remove most of the moisture. In addition, the test bed of the tunnel contains a heated plate so moisture would not resorb on the particles during pumpdown. The temperature of both the particles and the bed, however, was not sufficient to significantly alter the characteristics of the wind boundary layer, hence the Monin-Obukhov Length is infinite and the boundary layer may be considered neutral.

Another important parameter of the test particles is the distribution of particle sizes within each sample. Although only limited experiments with mixed particle size samples have been conducted, it is noted that the presence of a relatively few large grains can cause threshold at a much lower value than if the sample consisted of homogeneously-sized small grains, probably because of the increased surface roughness. Conversely, if a sample of intermediate-size particles contained a high frequency of tiny grains, then the overall threshold speed may be anomalously high. Thus care was taken to ensure relatively accurate size distributions for the test samples; nonetheless, it was not always possible to obtain well-graded samples.

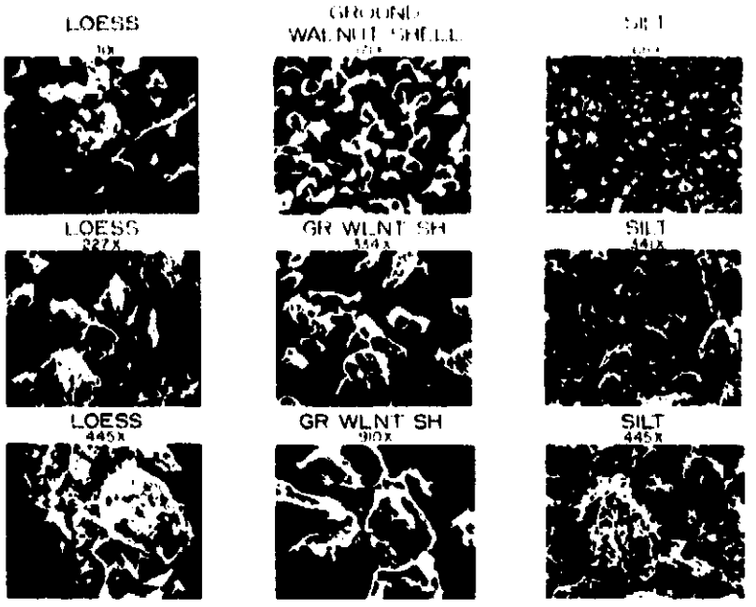

Figure 12.– Comparison of the shape of walnut shells with losses and water-deposited silt. The shape, degree of sorting, and cleanliness of the walnut shells is very similar to windblown losses.

Test bed length and threshold determination.– An important parameter in threshold tests is the length of the bed of material being tested (fig. 13). If the bed length was not sufficiently long, the experimental value of the threshold speed would be unrealistically high. If the bed length was longer than a critical length, the experimentally determined value of U'_{*t} became a constant. Furthermore, the critical minimum bed length is not constant for all particle diameters but appears to be a

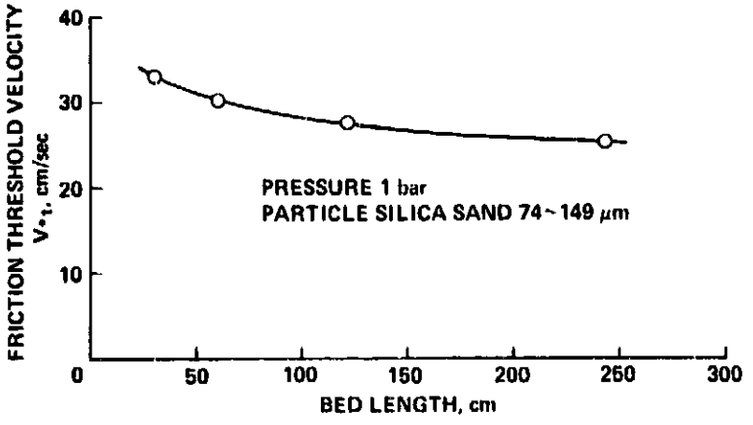

Figure 13.– Effect of length of particle test bed on threshold at 1 bar pressure for 74-149 μm silica sand. Lengths shorter than about 1.5 m result in anomalously high friction threshold.

function of the particle diameter and atmospheric pressure. For the smaller-sized particles the required critical bed length is substantially shorter than that for the larger-sized particles. For the major size ranges of test particles, a series of tests was run to determine the critical minimum bed length for the subsequent threshold tests. Typically a critical bed length of 2 m is needed for particles with diameters of 500 μm and about 1-m bed length for smaller particles.

Saltation threshold is defined here as occurring when grains of a given size are set into motion over an entire bed. High-speed motion pictures and direct observations showed that typically in the wind tunnel, as the wind is slowly increased, a speed is reached at which a few grains begin to quiver, roll, and saltate; this is followed by a flurry of activity, then by relatively no motion. This is not considered true threshold since it appears to be the result of the manner of emplacement of the particles on the test bed. Evidently there are some particles that are "perched" above the general surface and are highly susceptible to movement by the wind. Thus the procedure in the tunnel is to raise the wind speed to the point that these grains are removed, with the surface of the bed being repositioned naturally by the wind. The velocity is decreased below this initial movement then slowly increased until true saltation of the bed is observed. Several data points were taken at each pressure and several particle samples were tested two or more times in subsequent runs to determine repeatability of the data; the error band was found to be on the order of 20 percent.

Saltation can be detected by several methods. Previous threshold experiments (refs. 14, 18, and 19) conducted under one-atmosphere pressure involved visual observations of the entire test bed (saltation results in a cloud of particles moving over the entire surface) and observation of a ~2-cm-sized patch of the bed through a telescope. This procedure, however, is not practical in MARSWIT for low pressure experiments since the tunnel test bed is too far removed from the observation port of the control room (fig. 7). This saltation is detected by means of, first, a high resolution closed-circuit television system having a 1000-mm focal length camera lens to observe a patch of the test bed about 3 cm across; and second, a *laser beam-photometer system* (fig. 14) in which a laser beam is directed longitudinally down the test bed, reflected off a mirror at the end of the tunnel and directed back across the test bed where it activates a photocell. As soon as saltation occurs, the particles in motion interfere with the laser beam, causing less light to reach the photocell

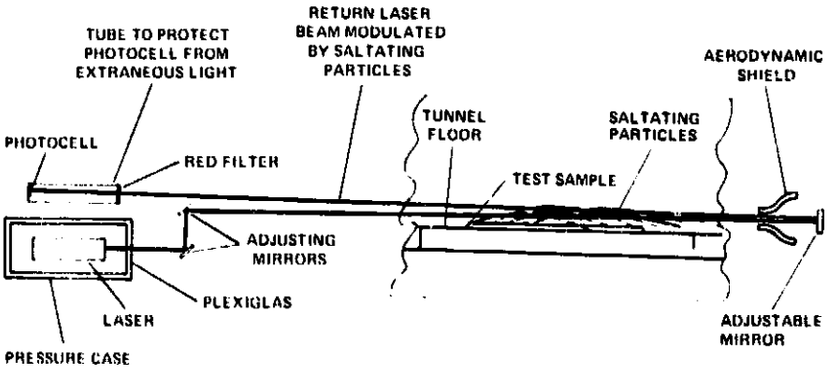

Figure 14. Schematic diagram showing laser-beam saltation threshold device. A laser beam is directed across the floor of the tunnel, immediately above the test particles, and reflected from a mirror onto a photocell. As soon as particles begin saltation, they interfere with the laser beam which is detected by the photocell.

and reducing the signal generated by the photocell. The third method involves the use of an electrometer. It has been found in the wind tunnel that beds of saltating particles build up substantial electrical charges. An electrometer probe placed at the end of the test bed shows a rapid buildup of charge as soon as saltating particles begin to impinge upon the probe. This multiple method of saltation detection (television observation, laser beam-photometer, and electrometer) is used for both atmospheric and low pressure tests for uniformity in detection.

Threshold as a Function of Reynolds Number

Several recent calculations of saltation parameters (primarily threshold friction speeds) for Mars have been based on Bagnold's (ref. 21) terrestrial work. Many of these estimates (refs. 27--29, and others) are based on the assumption that Bagnold's coefficient A is a unique function of the particle friction Reynolds number B (i.e., $A = A(B)$). If A were a "universal" function of B, then one curve should suffice for all conditions, including various atmospheric pressures. This would allow fairly direct extrapolations from experiments conducted at one atmosphere to low atmospheric pressures such as Mars. However, parameters such as interparticle forces resulting from cohesion by adsorbed water or electrostatic charges which may be functions of atmospheric pressure would severely complicate the extrapolation.

In a recent report, Sagan and Bagnold (ref. 30) argue that since Mars is comparatively "dry," interparticle forces resulting from cohesion by absorbed water would be negligible. They assume that A is a certain function of Reynolds number B, but their function is not derived from Bagnold's original experimental curve. Instead, they present a curve for air extrapolated from the experimental threshold data of White (ref. 31) for particles in water. Since it is presumed that particles immersed in water are cohesionless (at least, as might be related to adsorbed moisture), their threshold curve for air is an estimate for cohesionless particles and deviates considerably from Bagnold's original curve for particles in air of diameter less than 100 μm. They present a threshold friction velocity curve for Mars in which there is no upturn in friction velocities for the smaller particles (ref. 30). However, with the return of Viking Lander pictures (fig. 3) showing rather cohesive, fine grained materials, Sagan agrees (personal communication) that some form of interparticle force must exist for small particles on Mars. In addition, as pointed out by Pollack *et al.* (ref. 17), the frictionless case of Sagan and Bagnold would predict particle motion to be much more frequent than is known to be the case from Viking results.

To determine the effect of interparticle force on threshold, Iversen *et al.* (ref. 19) conducted one-atmosphere wind-tunnel experiments for particles with specific gravities ranging from 0.21 to 11.35 and diameters ranging from 8 μm to 1290 μm, giving a wide range of particle friction Reynolds numbers. These results were combined with the limited threshold data obtained at low pressure by Weinberger and Adlon (ref. 32), and it was found that the "universality" of $A(B)$ for small particles at low pressure was essentially invalid.

Experimental Results Obtained Under Low Atmospheric Pressure

Initial results for friction threshold speeds conducted under low atmospheric pressure are presented in reference 15. The results presented here are expansions of those results and refinements to take into account such factors as the influence of bed length on threshold.

TABLE 1. - MATERIALS USED IN LOW PRESSURE THRESHOLD EXPERIMENTS

Material	Size, μm	Specific gravity
Calcite	6 - 200	2.7
Copper	12 - 60	8.9
Cork	175 - 850	0.27
Glass microspheres	5 - 710	2.47
Instant tea	400 - 1200	0.21
Polystyrene DVB	175 - 850	1.01
Sand	20 - 1400	2.67
Silt	<5 - 60	2.65
Walnut shell	<20 - 1400	1.34

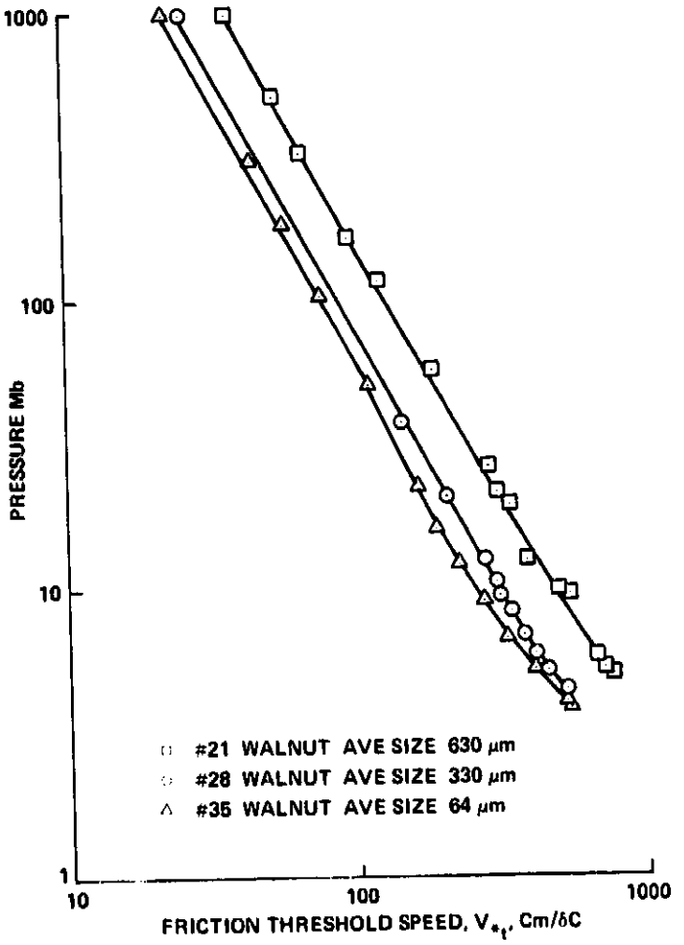

Figure 15.– Curve showing increase in friction threshold speed (V_{*_t}) with decrease in pressure.

For each sample material tested (table 1), threshold experiments were performed under pressures ranging from 4 mb (400 Pa) to 1000 mb (10^5 Pa). Figure 15 shows the threshold velocity as a function of atmospheric pressure for three samples of walnut shells, sizes 64 μm, 330 μm, and 630 μm. Similar graphs were obtained for each sample material. Values of V_{*_t} were taken from these graphs for each particle diameter to derive V_{*_t} vs D_p curves for several given atmospheric pressures (fig. 16).

A curve for demonstrating the functional relationship between A and B and its "nonuniversality" at different pressures is the dimensionless friction speed: $V_{*_t}[(\rho/\rho_p - \rho)g\nu]^{1/3} = (A^2B)^{1/3}$ vs dimensionless diameter: $D_p[(\rho_p - \rho)g/\rho\nu^2]^{1/3} = (B/A)^{2/3}$ (ref. 19). Figure 17 is such a plot for the ground walnut shells. The existence of separate curves for each of the diameters indicates the presence of additional terms (i.e., interparticle forces, etc.) in the functional relations and confirms the existence of the "upturn" in threshold curve for Mars with the corresponding existence of an "optimum" grain size for Mars.

Not all of the parameters (e.g., viscosities and temperatures) involved in aeolian movement can be satisfied in wind-tunnel simulations conducted on Earth, even under low-pressure conditions. Thus a combination of theory and wind-tunnel results must be employed for extrapolation to Mars as discussed in reference 15. Figure 18 shows threshold results performed at low pressure but with Earth air; figure 16 is an extrapolation of the wind-tunnel results to Mars based on the expressions derived by Iversen *et al.* (ref. 19), using the

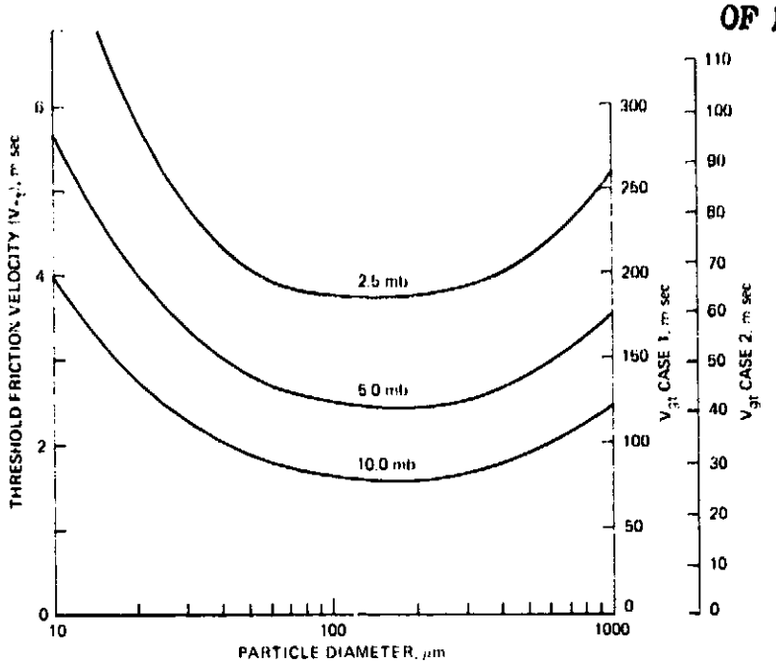

Figure 16.– Martian particle threshold curves as a function of particle size at three pressures. Scale on left is V_{*_t} in m/sec, two scales on right are equivalent free-stream (above the boundary layer) wind velocities (V_{gt}), based on atmospheric models by Pollack et al. (refs. 16 and 17). Case 1 is for winds blowing over a flat smooth surface composed of erodible grains; Case 2 is for a surface containing cobbles and small boulders.

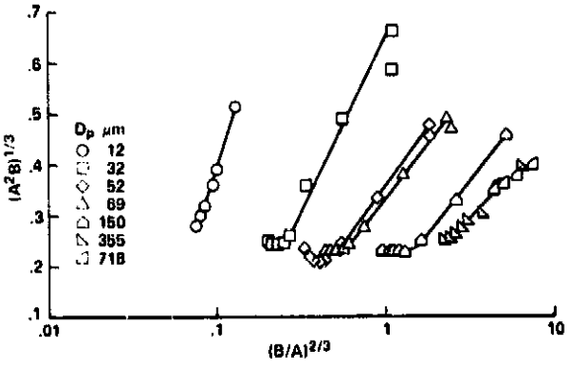

Figure 17.– Dimensionless threshold friction speed as a function of dimensionless particle diameter for several different ground walnut shell distribution. Experiments were performed from a minimum pressure of 5 mb to 1 atm. If Bagnold's A is uniquely only a function of B for nonterrestrial conditions, then only a single curve should suffice to fit all the data. Obviously, this is not the case, as each separate particle diameter range exhibits its own curve and $A = A(B)$ is not true when the pressure is varied. However, at a constant pressure, $(A^2B)^{1/3}$ is a unique function of $(B/A)^{2/3}$. The differences that occur owing to pressure changes may possibly be explained by changing of electrostatic and interparticle cohesive forces.

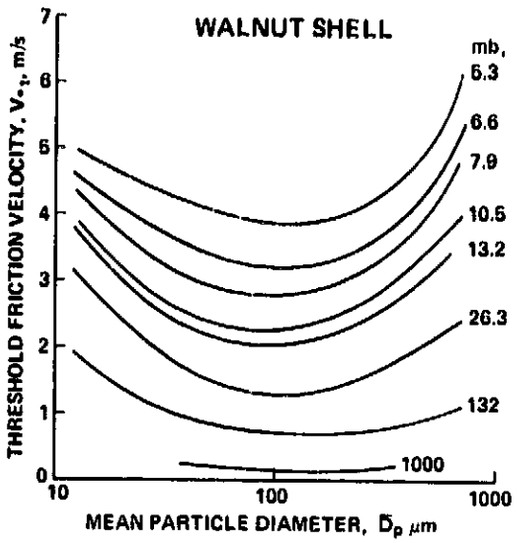

Figure 18.– Threshold friction velocities of particle diameter for walnut shells (circles) in Earth air at low pressure, compared to theoretical threshold curves, calculated using Earth air and Earth gravity to simulate the conditions.

appropriate values for kinematic viscosity and density for the martian atmosphere.

Minimum threshold friction speed (V_{*_t}) to move particles on Mars is about 2.5 m/sec. Depending upon the atmospheric conditions (ref. 17), at a nominal martian surface pressure of 5 mb (500 Pa) this would correspond to a wind velocity a couple of meters above the surface of about 125 m/sec for a smooth flat surface without boulders, or to about 43 m/sec for a surface with boulders (ref. 15).

The particle size most easily moved on Mars by the wind is about 160 μm in diameter as shown in figure 16. In an active wind regime over an area of relatively fixed particle formation, this size particle (fine sand) would be easily mobilized and eventually removed, either leaving behind both finer (silt) and coarser materials, or possibly causing the silt to go into suspension, depending on the ratio of sand to silt and their relative placement with respect to the wind.

OTHER PARAMETERS AFFECTING AEOLIAN PROCESSES ON MARS

The wind speeds needed to raise particles on Mars discussed under "Threshold Friction Speed Experiments" apply to relatively steady winds blowing across flat smooth plains consisting of loose, uniformly size-graded particles. The series of experiments to obtain V_{*_t} for these parametrically simple but probably unrealistic conditions, was a first-order analysis in which the number of factors was kept to a minimum. It is obvious from the Viking Lander pictures that for at least two localities on Mars, the surface is very complex; Viking Orbiter pictures indicate that the rest of the planet is equally or more complex.

In this section we will discuss some of the complicating factors that would alter the values of wind speeds needed to raise particles beyond those described above. In general, these effects lower the free-stream wind speeds needed to set particles into motion; however, very little research has been conducted on these effects, particularly in regard to low atmospheric pressure conditions, and the results presented here are exploratory in nature and should be taken as preliminary.

Swirling Motion Threshold

Many authors (e.g., ref. 33 and others) have recognized the difficulty of producing sufficiently high free-stream winds to raise particles on Mars. They have suggested that "dust-devil" or similar cyclonic-type winds may play an important or even dominant role in initiating martian dust storms.

In order to assess the relative effectiveness of swirling motion winds as a means of achieving particle threshold, a series of exploratory experiments was conducted at one atmosphere pressure to determine the strength and size of vortices needed to lift erodible particles (table 2) from the surface. Research involving a vortex generator (ref. 34) has been conducted at the Iowa State University Aerospace Engineering Department for the past several years. The vortex, formed with its axis perpendicular to the ground or surface plane, is produced by passing air through a rotating honeycomb and stationary nozzle located some distance above the surface. A vortex can be formed by passage of air either upwards or downwards through the honeycomb or with no air passage at all. The vortex formed is an approximate small-scale model of atmospheric vortices such as the tornado or dust-devil (fig. 19).

The swirling motion due to the atmospheric vortex (dust-devil) causes a radial pressure gradient at the surface

$$\frac{dp}{dr} = \frac{\rho u^2 \theta}{r} \sim \rho r \omega_0^2 \qquad (4a)$$

or

$$\rho \frac{u_\theta^2}{r} \Delta r \cong \Delta p = \rho r_0^2 \omega_0^2 \qquad (4b)$$

or

$$r_0 = \left(\frac{\Delta p}{\rho \omega_0^2} \right)^{1/2}$$

where p is pressure, r is radial distance from the vortex center, ρ is air density, u_θ is tangential (swirl) speed, ω_0 is the angular speed of the generator honeycomb, and the characteristic radius r_0 is as defined in equations (4) where Δp is the maximum surface pressure difference from the center of the vortex to that at large radius.

The maximum pressure difference, Δp, was measured on the surface plane of the vortex generator with a differential pressure transducer for the range of angular speeds ω_0 of the generator. The

TABLE 2. MATERIALS USED IN WIND-TUNNEL TESTS

Material	Density, ~gm/cm^3	Diameter, ~μm
Instant tea	0.21	719
Silica gel	0.89	17; 189
Nut shell	1.1	40 to 359
Clover seed	1.3	1290
Sugar	1.59	393
Glass	2.42	31 to 48
Glass	2.5	38 to 586
Sand	2.65	526
Aluminum	2.7	36 to 204
Glass	3.99	55 to 519
Copper oxide	6.0	10
Bronze	7.8	616
Copper	8.94	12; 37
Lead	11.35	8; 720

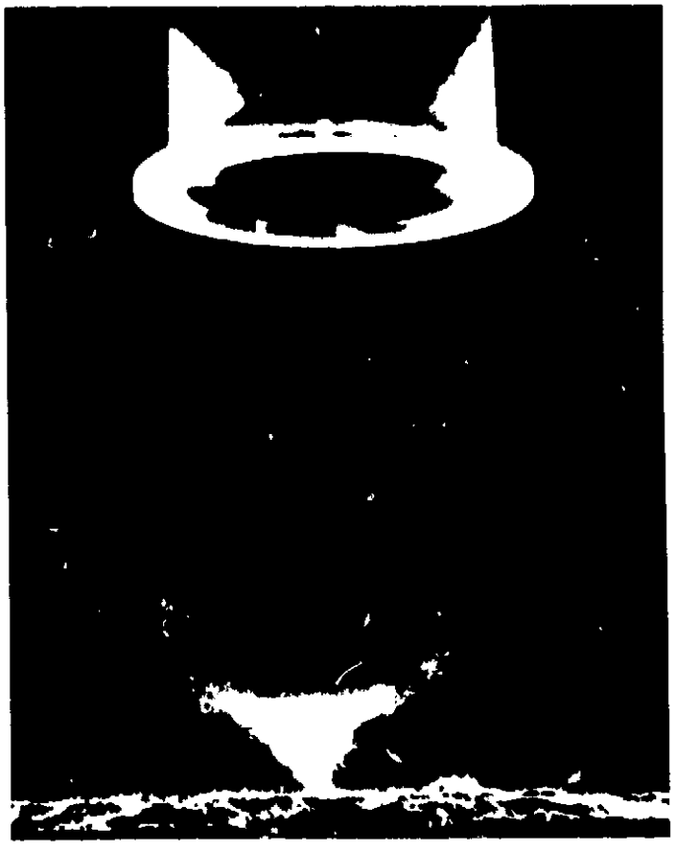

Figure 19.— View of the swirling (cyclonic) motion device, raising a small "dust devil" of particles above a test bed.

values of characteristic radius r_0 calculated from the measured values of Δp are shown in figure 20. A linear fit of the data results in an equation for r_0

$$r_0 = 0.0092\,\omega_0 + 6.87 \qquad (5)$$

where r_0 is in cm and ω_0 in rad/sec.

Assume that the top layer of particles of thickness equal to particle diameter D_p is lifted by the vortex at threshold. The forces acting on this layer per unit area are then as shown

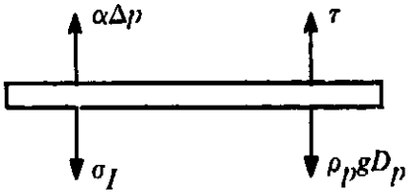

In the figure above, Δp represents the instantaneous pressure difference between the lower and upper surfaces of the particle layer, caused by the vortex moving over the part of the layer where particles are observed to lift off the surface. The factor α is included to account for pressure relief that might occur prior to particle lift-off; σ_I is the stress due to interparticle force, τ is an upward normal stress due to the effects of viscosity, $\rho_p g D_p$ is the weight of the particle layer per unit area, and α is an unknown constant of proportionality. If the upper layer were completely sealed α would be 1; if there were leakage α would be less than 1. If the surface stress τ is defined as $\tau = C_\tau \rho r_0^2 \omega_0^2$, then the value of $r_0\omega_0$ is threshold where forces are in equilibrium can be written as

$$r_0\omega_0 = \frac{1}{(\alpha + C_\tau)^{1/2}} \left(\frac{\rho_p g D_p}{\rho}\right)^{1/2} \left(\frac{1 + \sigma_I}{\rho_p g D_p}\right)^{1/2} \qquad (6)$$

The characteristic threshold speed $r_0\omega_0$ is not a true speed but is proportional to the square root of the pressure difference Δp (*i.e.*, $r_0\omega_0 = (\Delta p/\rho)^{1/2}$).

Unfortunately neither the function $\sigma_I(D_p)$ nor the function $C_\tau(r_0^2\omega_0/\tau)$ nor the ratio α are known, and sufficient data to determine these functions empirically is not yet available. The values of $r_0\omega_0$ at threshold are shown as a function of particle diameter in figure 21 and as a function of $(\rho_p g D_p/\rho)^{1/2}$ in figure 22. Figure 22 does show a trend for increasing angular threshold speed for

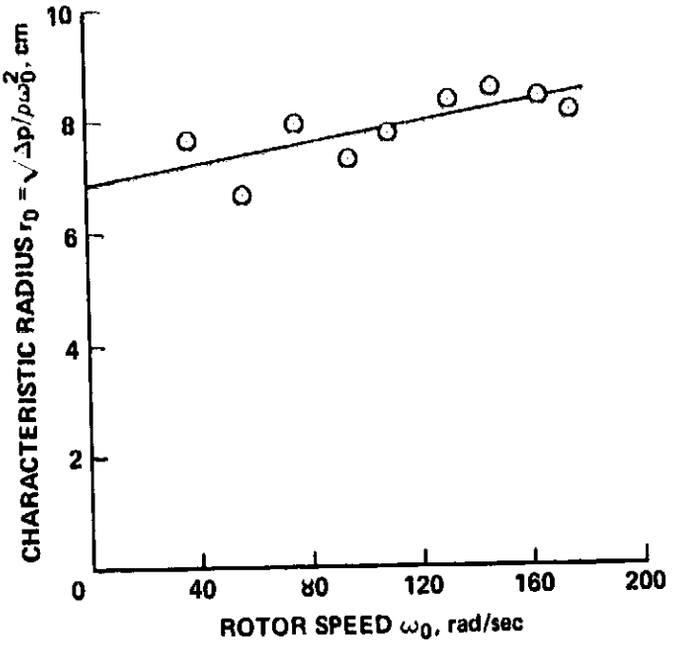

Figure 20.– Characteristic radius of the vortex as a function of rotor speed (see eqs. (4) and (5)).

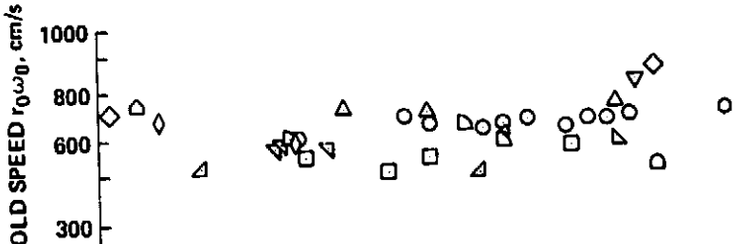

Figure 21.– Characteristic vortex threshold speed $r_0\omega_0$ as a function of particle diameter.

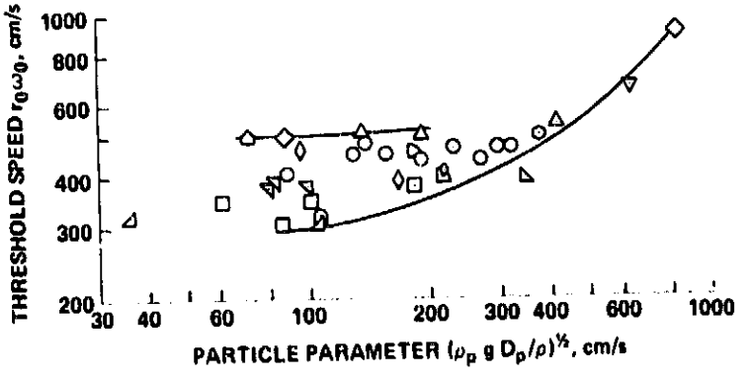

Figure 22.– Characteristic vortex threshold speed $r_0\omega_0 = (\Delta p/\rho)^{1/2}$ as a function of particle parameter. Note that for large particles the pressure difference Δp is nearly equal to the weight per unit area of a single layer of particles. For small particles the pressure difference Δp ranges up to nearly ten times the weight per unit area of a single layer. One explanation for the difference is small particle cohesion (interparticle stress σ_f).

larger values of this function. However, since the effects of Reynolds number $r_0^2 \omega/\nu$ and interparticle force are not accounted for, there is a large amount of data scatter for most of the range of the data.

The entrainment mechanism for raising surface particles with a vertical vortex (dust devil) is obviously quite different from the uniform wind boundary-layer case. The variation with particle diameter is much less pronounced for vortex threshold than it is for boundary-layer threshold. The important points to note from these exploratory experiments is that the size and density seem to have little importance in swirling motion threshold except for the two extreme cases of large lead and bronze particles. Thus cyclonic motion winds would appear to be very effective in raising erodible particles of all types and sizes. Once lifted above the surface, much lower winds than "normal" threshold could continue to carry particles along.

Behavior of Windblown Particles at Low Pressure

Once particles are set into saltation by the wind, their behavior at low pressure is quite different from that of particles under one atmosphere conditions. For example, because much stronger winds are required for threshold, the particles carried by the wind in saltation and suspension will also be moving faster after threshold. When they impact other particles and rock surfaces they will impart more energy to the impacted surface, which may result in a greater erosive capability at low pressure as well as potentially lowering the dynamic threshold of the impacted grains.

Moreover, partly because of the increased particle velocities and reduced atmospheric drag, the saltation path length has been calculated to be up to 50 times longer than on Earth, according to the assumed surface conditions. These values are based on numerical simulations, using wind-tunnel data obtained at one atmosphere surface pressure (ref. 5).

Since the geometry of ripple length, erosional scour patterns, and other aeolian features is dependent on the characteristics of the saltation trajectories, we should expect to see differences in these features on Mars. For example, Viking Lander photographs show a pronounced scour zone in the deposits of fine-grained particles around many of the rocks; although similar patterns develop around rocks on Earth, there appear to be geometric differences in the martian cases, primarily in the form of deeper and longer scour zones. This may be explained by the differences in the boundary layers near the surface. The properties of the viscous sublayer flow within the boundary layer influences the motion of the grains. On Earth, the typical range of saltation occurs when there is no viscous sublayer or at most a very minute one (~1 mm thick; ref. 5). The viscous sublayer is proportional to ν/u_* which can be up to 10 times as large as that on Earth or ~1 cm thick. Thus the effect is to have greater viscous interactions occurring at the surface on Mars and in the low pressure experiments, and the results are deeper erosion and extension of erosion further downstream.

To test potential causes of such differences, several experiments were conducted in MARSWIT. A rock about 12 cm across was placed in the tunnel on a bed of fine sand; under one atmosphere condition, the sand was eroded to determine the scour zones in relation to the rock. Vortices and turbulence around the rock resulted in eroded zones in front of the rock and off its leeward sides, a pattern to be expected from the horseshoe vortex flow field described (refs. 4 and 14). The same test was run under a surface pressure of 5.3 mb.

Although the basic pattern was the same for both cases (both result from horseshoe vortices), the erosion is more pronounced for the simulated martian case. Both cases were run at wind speeds slightly higher than threshold; because V_{*_f} is many times higher for martian conditions than for Earth conditions, the free-stream wind velocity is also considerably higher. The pressure differential acting on the particles is approximately the same, however. Once the particles are picked up by the wind, they also travel faster. When the saltating grains strike the rock, they bounce off the face of the rock with greater energies and erode the zone in front of the rock to a greater degree. Moreover, because the saltation path length is greater under martian conditions, as the grains are swept into the horseshoe vortex around the rock, they will strike the surface at a greater distance downwind from the rock than they did at one atmosphere. Such a result has the effect of lengthening the aeolian "shadow" zone behind rocks and other obstructions. Since the grains are traveling at a greater velocity and have a larger momentum, upstream grains are also less likely to be "captured" by the rock as they enter its flow field.

Another aspect of particle behavior at low pressure that affects threshold and may affect rates of erosion also, is the spin rate of grains in saltation. Although it has been known for some time that saltating grains are spinning, the significance of that fact has not been fully appreciated. For example, White and Schulz (ref. 20) have shown that part of the lift on the particle in the saltation trajectory is attributable to the Magnus effect resulting from spinning grains. As the particles begin to lift above the bed, they begin spinning due to shear forces in the boundary layer. Analysis of high-speed motion pictures of saltating grains show that they spin up to 200 rps under one atmosphere condition. Extrapolation to martian conditions show that spin rates are more than doubled, or about 450 rps. Although the effect of rapidly spinning grains on rates of erosion has not been assessed, it may be significant. Future experiments will utilize MARSWIT to test the rate of spin at low pressure as well as to assess the effect of spinning grains on rates of erosion.

SUMMARY AND CONCLUSIONS

That aeolian processes have played and continue to play a significant role in the evolution of the surface of Mars cannot be disputed. Unfortunately, aeolian processes on Mars are poorly understood, primarily because of the drastically different aeolian environment compared to Earth's; yet, without good knowledge of these processes, the geological history of Mars remains shadowed. Rates of aeolian erosion provide a case in point. Prior to the Viking mission, orbital pictures from Mariner 9 showed numerous features that were attributed to winds, including dunes, crater streaks, and other depositional features. Pedestal craters, yardangs, sculpted laminated terrain and other features observed from orbit prompted the general conclusion that vast regions had been eroded to significant depths by the wind. It was reasoned that the frequent dust storms and the postulated high winds would be capable of accomplishing high rates of erosion.

Viking results, however, are raising serious questions about just how much wind erosion has occurred. Pictures from orbit, for example, show that many of the pedestal craters are not erosional but are *primary* landforms — some are fresh impact craters (ref. 35) and others are probably volcanoes, although some still appear to result from erosion.

Viking Lander pictures in Chryse Planitia lead to the conclusion that the plains may have undergone from 1–10 m of surface erosion since their emplacement, a rather small amount

considering their great age as tentatively determined from crater counts (Binder, personal communication). Moreover, rocks visible in the Lander pictures show few of the surface textures and features expected from wind erosion, as least by terrestrial comparisons. Similar conclusions have been reached for the Viking II Lander site.

Other surprises from Viking are causing the questions about wind erosion on Mars to be reasked. The basic question is: How effective is wind erosion on Mars under the present environment, and how might it have been different in the past? To answer this question, one must know:

1. The range of wind speeds at which particles are driven by the wind.
2. The characteristics of saltation in the martian atmosphere.
3. The effects of electrostatically-charged particles.
4. Rock weathering in the martian environment.
5. Frequency-magnitude determinations of martian surface winds.

Solutions to these complex problems will undoubtedly take years to derive. Nonetheless, results presented here are focusing on these problems, which, when combined with analysis of spacecraft data will lead to a much clearer understanding of aeolian processes on Mars.

ACKNOWLEDGMENTS

The development of the Martian Surface Wind Tunnel (MARSWIT) involved the efforts of many individuals. We wish to acknowledge T. Brown, Facilities Engineering Section, NASA-Ames Research Center, for his initial design and H. Larson for his cooperation in the "pump-down" phase of the low pressure experiments.

Several students from the University of Santa Clara were instrumental in the design and operation of several components of the MARSWIT. We acknowledge Jeff Neiberg for the design and construction of the pressure sensor system to determine wind velocities, Dave Merrit for the design and construction of the control panel and other electrical components, and Gary Giampaoli for the design and construction of the high resolution television monitoring system.

This work is supported by the Office of Planetary Geology, National Aeronautics and Space Administration, through Grant NGR 05-017-037 to the University of Santa Clara and NASA-Ames Research Center, through Interchange Agreement NCA 2-OR 340-701 to Iowa State University and Interchange Agreement NCA 2-OR 180-605 to the University of California at Davis.

Ames Research Center
National Aeronautics and Space Administration
Moffett Field, California 94035, August 4, 1977

REFERENCES

1. Gierasch, Peter J.: Martian dust storms. Rev. Geophys. Space Phys., vol. 12, no. 4, 1974, pp. 730–734.

2. Sagan, Carl; Veverka, Joseph; Fox, Paul; Dubisch, Russell; Lederberg, Joshua; Levinthal, Elliott; Quam, Lynn; Tucker, Robert; Pollack, James B.; and Smith, Bradford A.: Variable Features on Mars: Preliminary Mariner 9 Television Results. Icarus, vol. 17, 1972, pp. 346–372.

3. Veverka, J.; Sagan, C.; Quam, Lynn; Tucker, R.; and Eross, B.: Variable features on Mars III: Comparison of Mariner 1969 and Mariner 1971 photography. Icarus, vol. 21, 1974, pp. 317–368.

4. Greeley, Ronald; Iversen, James D.; Pollack, James B.; Udovich, Nancy; and White, Bruce: Wind tunnel simulations of light and dark streaks on Mars. Science, vol. 183, no. 4127, 1974a, pp. 847–849.

5. White, Bruce R.; Greeley, Ronald; Iversen, James D.; and Pollack, James B.: Estimated grain saltation in a martian atmosphere. Jour. Geophys. Res., vol. 81, no. 32, 1976, pp. 5643–5650.

6. Iversen, J. D.; Greeley, R.; White, B. R.; and Pollack, J. B.: Aeolian erosion on the martian surface, Part 1: Erosion rate similitude. Icarus, vol. 26, 1975, pp. 321–331.

7. Iversen, J. D.; Pollack, J. B.; Greeley, R.; and White, B. R.: The effect of vertical distribution in the modeling of sedimentation phenomena: Martian crater wake streaks. J. Geophys. Res., vol. 81, 1976b, pp. 4846–4856.

8. Veverka, J.; Sagan, C.; and Greeley, R.: Variable features on Mars. VI. An unusual crater streak in Mesogaea. Icarus, vol. 27, 1976, pp. 241–253.

9. Mutch, Thomas A.; Binder, Alan B.; Huck, Friedrich O.; Levinthal, Elliott; Liebes, Sidney, Jr.; Morris, Elliot C.; Patterson, William R.; Pollack, James B.; Sagan, Carl; and Taylor, Glenn R.: The surface of Mars: The view from the Viking 1 lander. Science, vol. 193, no. 4255, 1976a, pp. 791–801.

10. Mutch, Thomas A.; Arvidson, Raymond E.; Binder, Alan B.; Huck, Friedrich O.; Levinthal, Elliott C.; Liebes, Sidney, Jr.; Morris, Elliot C.; Nummedal, Dag; Pollack, James B.; and Sagan, Carl: Fine particles on Mars: Observations with the Viking 1 Lander cameras. Science, vol. 194, no. 4260, 1976b, pp. 87–91.

11. Carr, Michael H.; Masursky, Harold; Baum, William A.; Blasius, Karl R.; Briggs, Geoffrey A.; Cutts, James A.; Duxbury, Thomas; Greeley, Ronald; Guest, John E.; Smith, Bradford A.; Soderblom, Laurence A.; Veverka, Joseph; and Wellman, John B.: Preliminary Results from the Viking Orbiter Imaging Experiment. Science, vol. 193, no. 4255, 1976, pp. 766–776.

12. Hess, S. L.; Henry, R. M.; Leovy, C. B.; Ryan, J. A.; Tillman, J. E.; Chamberlain, T. E.; Cole, H. L.; Dutton, R. G.; Greene, G. C.; Simon, W. E.; and Mitchell, J. L.: Preliminary meteorological results on Mars from the Viking 1 lander. Science, vol. 193, no. 4255, 1976a, pp. 788–791.

13. Hess, S. L.; Henry, R. M.; Leovy, C. B.; Ryan, J. A.; Tillman, J. E.; Chamberlain, T. E.; Cole, H. L.; Dutton, R. G.; Greene, G. C.; Simon, W. E.; and Mitchell, J. L.: Mars climatology from Viking 1 after 20 sols. Science, vol. 194, no. 4260, 1976b, pp. 78–81.

14. Greeley, J.; Iversen, J. D.; Pollack, J. B.; Udovich, Nancy, and White, B.: Wind tunnel studies of martian aeolian processes. Proc. R. Soc. London A., vol. 341, 1974b, pp. 331–360.

15. Greeley, R.; White, B.; Leach, R.; Iversen, J.; and Pollack, J.: Mars: Wind friction speeds for particle movement. Geophysical Research Letters, vol. 3, no. 8, 1976, pp. 417–420.

16. Pollack, James B.; Haberle, Robert; Greeley, Ronald; and Iversen, James: Estimates of the wind speeds required for particle motion on Mars. Icarus, vol. 29, 1976a, pp. 395–417.

17. Pollack, James B.; Leovy, Conway B.; Mintz, Yale H.; and VanCamp, Warren: Winds on Mars during the Viking season: Predictions based on a general circulation model with topography. Geophys. Res. Letters, vol. 3, no. 8, 1976b, pp. 479–482.

18. Iversen, J. D.; Greeley, R.; Pollack, J. B.; and White, B. R.: Simulation of martian aeolian phenomena in the atmospheric wind tunnel. NASA SP-336, 1973, pp. 191–213.

19. Iversen, J. D.; Pollack, J. B.; Greeley, R.; and White, B. R.: Saltation threshold on Mars: The effect of interparticle force, surface roughness, and low atmospheric density. Icarus, vol. 29, 1976a, pp. 381–393.

20. White Bruce R.; and Schulz, Jan C.: Magnus effect in saltation. Journal of Fluid Mechanics, vol. 81, no. 3, 1977, pp. 497–512.

21. Bagnold, Ralph A.: The Physics of Blown Sand and Desert Dunes. W. Morrow & Co., N.Y., 1942.

22. Owen, Tobias, and Biemann, K.: Composition of the atmosphere at the surface of Mars: Detection of Argon-36 and preliminary analysis. Science, vol. 193, no. 4255, 1976, pp. 801–803.

23. Shorthill, Richard W.; Hutton, Robert E.; Moore, Henry J., II; Scott, Ronald F.; and Spitzer, Cary R.: Physical properties of the martian surface from the Viking 1 Lander: Preliminary results. Science, vol. 193, no. 4255, 1976a, pp. 805–809.

24. Shorthill, Richard W.; Moore, Henry J., II; Scott, Ronald F.; Hutton, Robert E.; Liebes, Sidney, Jr.; and Spitzer, Cary R.: The "Soil" of Mars (Viking 1). Science, vol. 194, no. 4260, 1976b, pp. 91–97.

25. Hargraves, R. B.; Collinson, D. W.; and Spitzer, C. R.: Viking magnetic properties investigation: Preliminary results. Science, vol. 194, no. 4260, 1976, pp. 84–86.

26. Pollack, J. B.; Colburn, D.; Kahn, R.; Hunter, J.; VanCamp, W.; Carlston, C. E.; and Wolfe, M. R.: Properties of aerosols in the martian atmosphere as inferred from Viking Lander imaging data. J. of Geophysical Research, vol. 82, no. 28, 1977, pp. 4479–4496.

27. Ryan, J. A.: Notes on the martian yellow clouds. J. Geophys. Res., vol. 69, 1964, pp. 3759–3770.

28. Sagan, Carl; and Pollack, James B.: 1969. Windblown dust on Mars. Nature, vol. 223, 1969, no. 5208, 1969, pp. 791–794.

29. Hess, S. L.: Martian winds and dust clouds. Planet. Space Sci., vol. 21, 1973, pp. 1549–1557.

30. Sagan, Carl; and Bagnold, R. A.: Fluid transport on Earth and aeolian transport on Mars. Icarus, vol. 26, 1975, pp. 209–218.

31. White, S. J.: Plane bed thresholds of fine grained sediments. Nature, vol. 228, no. 5267, pp. 152–153.

32. Adlon, G. L.; and Weinberger, R. K.: Particle dislodgement and entrainment by a low density airstream flowing over a surface. NASA CR-111924, 1972.

33. Gierasch, P. J.; and Goody, R. M.: A model of a martian great dust storm. J. Atmospheric Sciences, vol. 30, no. 2, 1973, pp. 169–179.

34. Hsu, C. T.; and Fattahi, B.: Tornado funnel formation from a tornado cyclone. Proc. 9th Conf. on Severe Local Storms, American Meteorological Society, Norman, Okla., Oct. 1975.

35. Carr, M. H.; Crumpler, L. A.; Cutts, J. A.; Greeley, R.; Guest, J. E.; and Masursky, H.: Martian impact craters and emplacement of ejecta by surface flow. J. Geophysical Research, vol. 82, no. 28, 1977, pp. 4039–4054.

36. Iversen, J. D.; Greeley, R.; and Pollack, J. B.: Windblown dust on Earth, Mars, and Venus. J. Atmos. Sci., vol. 33, no. 12, 1976c, pp. 2425–2429.

1. Report No.	2. Government Accession No.	3. Recipient's Catalog No.
NASA TM-78,423		

4. Title and Subtitle	5. Report Date
DUST STORMS ON MARS: CONSIDERATIONS AND SIMULATIONS	December 1977
	6. Performing Organization Code

7. Author(s)	8. Performing Organization Report No.
Ronald Greeley,* Bruce R. White,† James B. Pollack,‡ James D. Iverson,§ and Rodman N. Leach*	A-7152
	10. Work Unit No. 384-47-66-03
9. Performing Organization Name and Address	11. Contract or Grant No.
*University of Santa Clara, NASA Ames Research Center, Moffett Field, Calif. 94035 †Mechanical Engineering Department, University of California, Davis, Calif. 95616 ‡NASA Ames Research Center, Moffett Field, Calif. 94035 §Department of Aerospace Engineering, Iowa State University, Ames, Iowa 50010	
	13. Type of Report and Period Covered Technical Memorandum
12. Sponsoring Agency Name and Address National Aeronautics and Space Administration Washington, D.C. 20546	14. Sponsoring Agency Code

15. Supplementary Notes

Submitted to the Proceedings of the Desert Dust Symposium, (T. J. Pewe, Editor) American Association for the Advancement of Science, Denver Meeting, 1977.

16. Abstract

Aeolian processes are important in modifying the surface of Mars at present, and appear to have been significant in the geological past. Aeolian activity includes local and global dust storms, the formation of erosional features such as yardangs and depositional features such as sand dunes, and the erosion of rock and soil. As a means of understanding aeolian processes on Mars, an investigation is in progress that includes laboratory simulations, field studies of Earth analogs, and interpretation of spacecraft data. This report describes the Martian Surface Wind Tunnel (MARSWIT), an experimental facility established at NASA-Ames Research Center, and presents some results of the general investigation. Experiments dealing with wind speeds and other conditions required for the initiation of particle movement on Mars are described and considerations are given to the resulting effectiveness of aeolian erosion.

17. Key Words (Suggested by Author(s))	18. Distribution Statement
Mars, Aeolian processes Mars geology Viking Mars erosion Mars dust	Unlimited STAR Category 91

19. Security Classif. (of this report)	20. Security Classif. (of this page)	21. No. of Pages	22. Price*
Unclassified	Unclassified	30	$4.00

*For sale by the National Technical Information Service, Springfield, Virginia 22161

NASA-Langley, 1977